Since January 2020 Elsevier has created a COVID-19 resource centre with free information in English and Mandarin on the novel coronavirus COVID-19. The COVID-19 resource centre is hosted on Elsevier Connect, the company's public news and information website.

Elsevier hereby grants permission to make all its COVID-19-related research that is available on the COVID-19 resource centre - including this research content - immediately available in PubMed Central and other publicly funded repositories, such as the WHO COVID database with rights for unrestricted research re-use and analyses in any form or by any means with acknowledgement of the original source. These permissions are granted for free by Elsevier for as long as the COVID-19 resource centre remains active.

Nano Energy 74 (2020) 104910

Contents lists available at ScienceDirect

Nano Energy

journal homepage: http://www.elsevier.com/locate/nanoen

Distributed mobile ultraviolet light sources driven by ambient mechanical stimuli

Zhaozheng Wang [a,b,1], Yunxu Shi [b,1], Fan Liu [a], Hao Wang [a], Xu Liu [a], Runtong Sun [a], Yijia Lu [a], Linhong Ji [a], Zhong Lin Wang [c,d,**], Jia Cheng [a,*]

[a] State Key Laboratory of Tribology, Department of Mechanical Engineering, Tsinghua University, Beijing, China
[b] School of Electromechanical and Automotive Engineering, YanTai University, Shandong, China
[c] Beijing Institute of Nanoenergy and Nanosystems, Chinese Academy of Sciences, Beijing, 100083, China
[d] School of Materials Science and Engineering, Georgia Institute of Technology, Atlanta, GA, 30332-0245, USA

ARTICLE INFO

Keywords:
Triboelectric nanogenerators
Ultraviolet light
High voltage application

ABSTRACT

Due to the natural characteristics of high voltage output, Triboelectric Nanogenerators (TENGs) have huge advantages in many fields. Here, we have proposed a concept of Mobile ultraviolet light sources (Mobile-UV) driven by TENG, without any additional circuits. For this system, analysis of electric characteristics, optical emission spectra, and COMSOL simulation were carried out to promote the performance. Subsequently, we have developed exploratory applications in the fields of bio-sterilization, chemical detection, and UV-curing, which proved the versatility and effectiveness. This work offers a promising, portable, effective, and safe supplement to traditional ultraviolet light sources, and will enrich the diversity of the ultraviolet application based on the reach of existing technologies.

1. Introduction

In many wild and poverty areas, drinking water sterilization and wound disinfection are urgent problems. There are still around one billion people without electricity in the world, especially in sub-Saharan Africa where the rate of access to electricity is only 44.6% [1,2]. Many plagues are also caused by water pollution or wound infection that cannot be disinfected in time. At present, common methods for disinfecting drinking water in the wild include electrochemistry [3,4], chlorine [5,6], bleach [7], boiling disinfection [8,9], etc. Most of these disinfections might cost too much time or cause secondary pollution, resulting in the poor quality of drinking water. In recent years, ultraviolet sterilization has become getting more popular as a new sterilization technology, especially it has the characteristics of fast sterilization and no secondary pollution. In addition, ultraviolet light has a large number of applications in medical treatment [10,11], chemical testing [12], etc., but its dependence on the power grid makes it almost impossible to use in areas without electricity or in the wild. Of course, the application of ultraviolet light in the industrial field should not be ignored. With the development of emerging light curing technologies such as UV-curing 3D printing, electronic packaging, dyeing [13–15], the application of ultraviolet rays will spread all over the industry. At present, there are mainly two ways to generate ultraviolet rays: One is a UV-LED lamp, it cannot meet the requirements on many occasions due to the short device life as a result of heat dissipation and immature technology. Another method is to use Ar–Hg lamp to produce ultraviolet light, but the lighting excited condition requires a high voltage of above 800 V. A common solution is to attach a complex boost circuit with AC 220 V which makes UV technology difficult to apply in areas without electricity. Therefore, a grid-independent UV sources is very promising and urgent for the market, especially in poor areas such as Africa.

At present, people often use natural energy to obtain electricity in poor areas or a wild environment. The method of using solar power is often inefficient because of the complex and varied weather. Using wind and water to convert mechanical energy into electrical energy has become a more common and efficient method. However, most of the methods are currently used to directly charge the battery for storing electrical energy. If it is used to generate ultraviolet light, a complex

* Corresponding author.
** Corresponding author. Beijing Institute of Nanoenergy and Nanosystems, Chinese Academy of Sciences, Beijing, 100083, China.
E-mail addresses: zhong.wang@mse.gatech.edu (Z.L. Wang), chengjia@tsinghua.edu.cn (J. Cheng).
[1] These authors contributed equally to this work.

https://doi.org/10.1016/j.nanoen.2020.104910
Received 23 March 2020; Received in revised form 23 April 2020; Accepted 28 April 2020
Available online 4 May 2020
2211-2855/© 2020 The Author(s). Published by Elsevier Ltd. This is an open access article under the CC BY license (http://creativecommons.org/licenses/by/4.0/).

boost circuit should be needed which will lead to a great attenuation of efficiency due to the power consumption of components in the boost circuit.

Recently, as a new power technology, triboelectric nanogenerators (TENGs) [16] have shown huge significance and application prospects in many fields, such as energy harvesting [17–25], blue energy [26–31], self-power sensors [32–46] and so on. In particular, more and more attention has been paid to the high voltage application of TENG, because the natural high voltage characteristics of TENG have shown great advantages in many fields, such as generating microplasma [47,48], field emission of electrons [49], quantitatively generating the input ions in mass spectrometry [50], Electrohydrodynamic Jet Printing [51], electro-assisted cell printing [52] and so on. Therefore, it is an ingenious and effective method to directly generate ultraviolet by TENG utilizing its high voltage characteristics. Previously, Chi Zhang et al. realized that generating ultraviolet radiation by the effect of triboelectric between PTFE and the glass chamber wall. Its mechanism is utilizing Ar discharge to stimulate mercury atom, which could produce the ultraviolet [53]. However, it can only produce in-situ ultraviolet radiation according to its structure and principle, which will greatly limit the application of ultraviolet radiation in space, especially in those areas where the position and angle of light need to be changed. (The systematical comparison of Water sterilization technology by TENG is presented in Supplementary note 1).

In this paper, we have developed Mobile ultraviolet light sources (Mobile-UV) light sources. This system generated ultraviolet light by generating a glow reaction under high pressure driven by the TENG. Firstly, the electrical and optical characteristics of the Mobile-UV were simultaneously analyzed. The effects of design parameters on the intensity of ultraviolet radiation were intensive studied, such as TENG speed, length, or diameter of the Mobile-UV tube. It could guide optimization in the future. In addition, Argon glow discharge performance in Mobile-UV tube directly affects ultraviolet generation, in order to further analyze the characteristic of glow discharge, the electron temperature and density of glow discharge were explored through the comparison of simulation and experiment. Finally, the versatility and practicability of the system were verified by the preliminary application of the Mobile-UV in the fields of bio-sterilization, chemical detection, and UV-curing. We believe that the Moblie-UV system will show tremendous innovations in the generation approaches and application scenarios of ultraviolet radiation, especially for the application of ultraviolet radiation in a large number of areas of no or poor electricity.

2. Results and discussion

2.1. Schematic and luminescence photograph of Mobile-UV

The key components of the Mobile-UV system are TENG and UV tube. The breakdown-voltage for Ar–Hg vapor to generate ultraviolet radiation is extremely high, above 800V. According to this condition, the freestanding rotary (FR) TENG structure is selected to power for the whole system. As the core component of the Mobile-UV system, the UV reactor has been designed and improved for different applications. The concept of the whole Mobile-UV system and its preliminary verification in related fields are shown in Fig. 1 (a). As a special form of freestanding triboelectric-layer mode, the operating mechanism of FR-TENG shows in Fig. 1 (b), the rotor of FR-TENG is acrylic covered with PVC film. In order to reduce the wear rate of FR-TENG and optimize the contact area between rotor and stator, the PVC film is designed as a floating structure; the stator is covered with nylon film based on copper plating on Printed Circuit Board (PCB). It is noteworthy that the output electrodes of FR-TENG are directly connected with the two electrodes of the UV tube. Compared with the traditional mode of driving the ultraviolet Ar–Hg lamp, the Mobile-UV has a simple structure and can be lighted without additional complex boost circuits. Fig. 1 (c) shows the detailed photograph and luminescence patterned of Mobile-UV tube directly driven by FR-TENG. The Non-luminescence patterned is shown in Supplementary note 2. The luminescence process of the patterned tube is shown in Supplementary Movie 1.

Supplementary video related to this article can be found at https://doi.org/10.1016/j.nanoen.2020.104910

2.2. Electric characteristics of Mobile-UV

In order to further analyze the characteristics of Mobile-UV and optimize the emission efficiency of ultraviolet radiation. Firstly, the

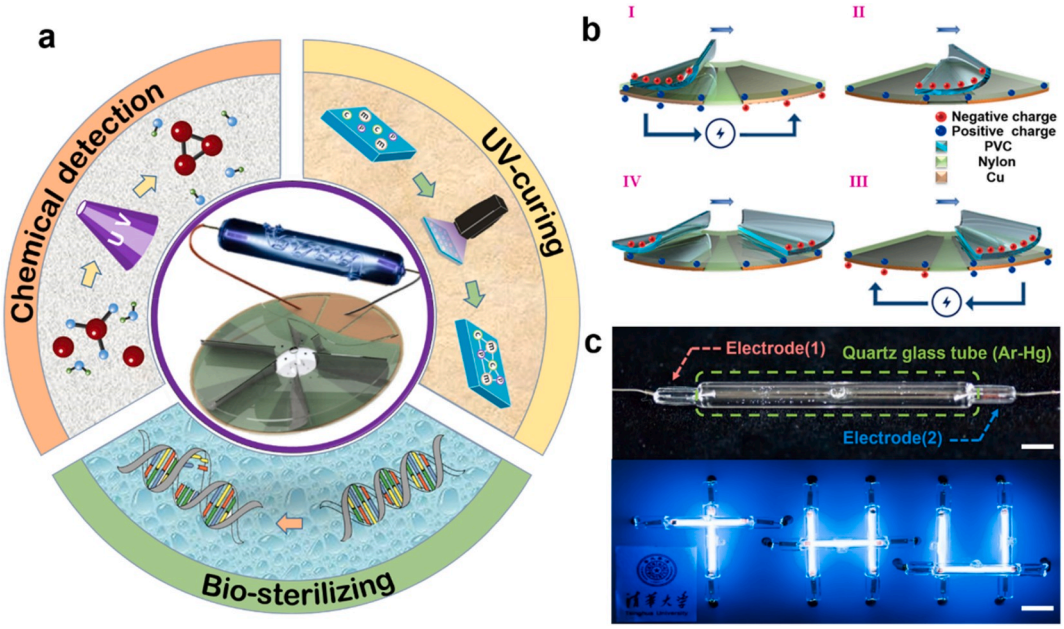

Fig. 1. Schematic and luminescence photographs of Mobile ultraviolet light sources (Mobile-UV). (a). Schematic and application fields of the Mobile-UV. (b). The working principle of freestanding rotary (FR) TENG. (c). The detail photograph (scale bar, 10 mm) and luminescence patterned (scale bar, 20 mm) of Mobile-UV tube directly driven by FR-TENG, no Photoshop (NIKON D700 @ 56 mm, ISO 640, f/6.3, 2 s exposure).

electric characteristics of FR-TENG are tested in detail. As shown in Fig. 2 (a) (b). The output performance of open-circuit voltage (V_{OC}) and short-circuit current (I_{SC}) of 12 units FR-TENG at different rotational speeds is tested, From Fig. 2 (c), it can be seen that the Voc is a little different. The 6 units one has the highest output voltage (about 4000 V at 400 RPM) instead of the 4 units one among these three structures. The discrepancy comes from the floating design of the rotator. Due to the toughness of the material, arched edge curling will occur with the increase of the rotator area, which leads to the reduction of the actual effective contact area. Fig. 2 (d) shows the more parts the FR-TENG has, the higher the short-circuit current is, due to the faster transferring of electrons. The highest Isc of FR-TENG with 12 units at 400 RPM is 233 μA. In addition, it can also be seen that the open-circuit voltage of 4,6,12 units ones are higher than 2000 V, which is far exceeding the discharge condition of the UV tube. As the current plays a more crucial role than the voltage in UV discharge, the 12 units structure with the highest current and a high enough voltage is adopted. The specific structure of FR-TENG is shown in Fig. 2 (e). As shown in Fig. 2 (f), an electrometer (Keithley 6514) for load current is connected in series in the circuit and another electrometer with high-voltage probe (HPV) is connected in parallel to measure the load voltage. The load electric experiment was carried out for a UV tube (with a diameter of 5 mm and a length of 50 mm). It can be seen from Fig. 2 (g) that under the drive of 12 units of FR-TENG, the effective value of load current increases with the increase of rotational speed. The maximum value appears at 400 RPM, reaching 110 μA. On the contrary, the effective value of load voltage decreases obviously with the increase of rotational speed. It is because the generation of UV light is a discharge process which will lead to a sudden drop in voltage. With the increase of rotational speed, the discharge frequency in the UV tube increases, resulting in a significant reduction in the effective value of voltage. The waveforms of the load voltage and load current are shown in **Supplementary note 3** in detail. Finally, the influence of load power with rotational speed was studied. Fig. 2 (h) shows that the load power of Mobile-UV will increase with the increase of rotational speed.

2.3. *Optical emission spectra of Mobile-UV*

Subsequently, the optical characteristic of Mobile-UV was quantitatively studied. Fig. 3 (a) shows the absolute spectral intensity of the Mobile-UV tube (with a diameter of 5 mm and a length of 50 mm) driven by FR-TENG at rotational speed from 100 to 400 RPM. It can be seen that with the increase of rotational speed, the absolute intensity of Mobile-UV increases linearly at 253 nm, reaching a maximum of 250.5 μW/cm^2/nm. UV sterilization band is usually in the range of 240–280 nm, the overwhelming majority of published papers on the effects of UV on

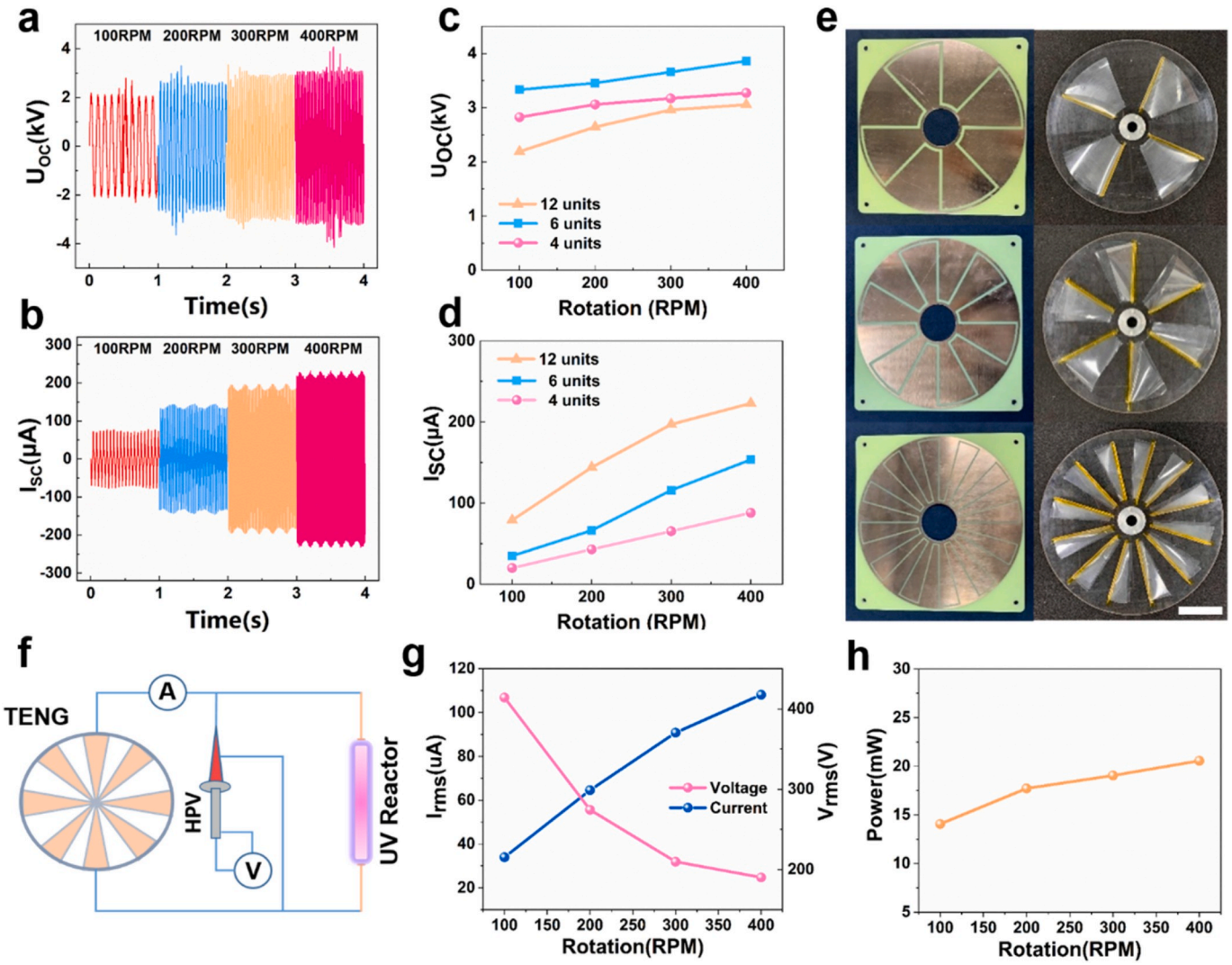

Fig. 2. Electric characteristics of FR-TENG and Mobile-UV. (a) (b). Open circuit voltage and short circuit current of FR-TENG with various rotational speeds. (c) (d). Open circuit voltage and short circuit current of different FR-TENG with various units. (e). The photos of FR-TENG structures for 4, 6, 12 units (scale bar, 80 mm). (f). Circuit schematic measuring electric characteristics of Mobile-UV. (g) (h). Load effective voltage, current and power of Mobile-UV with various rotational speeds.

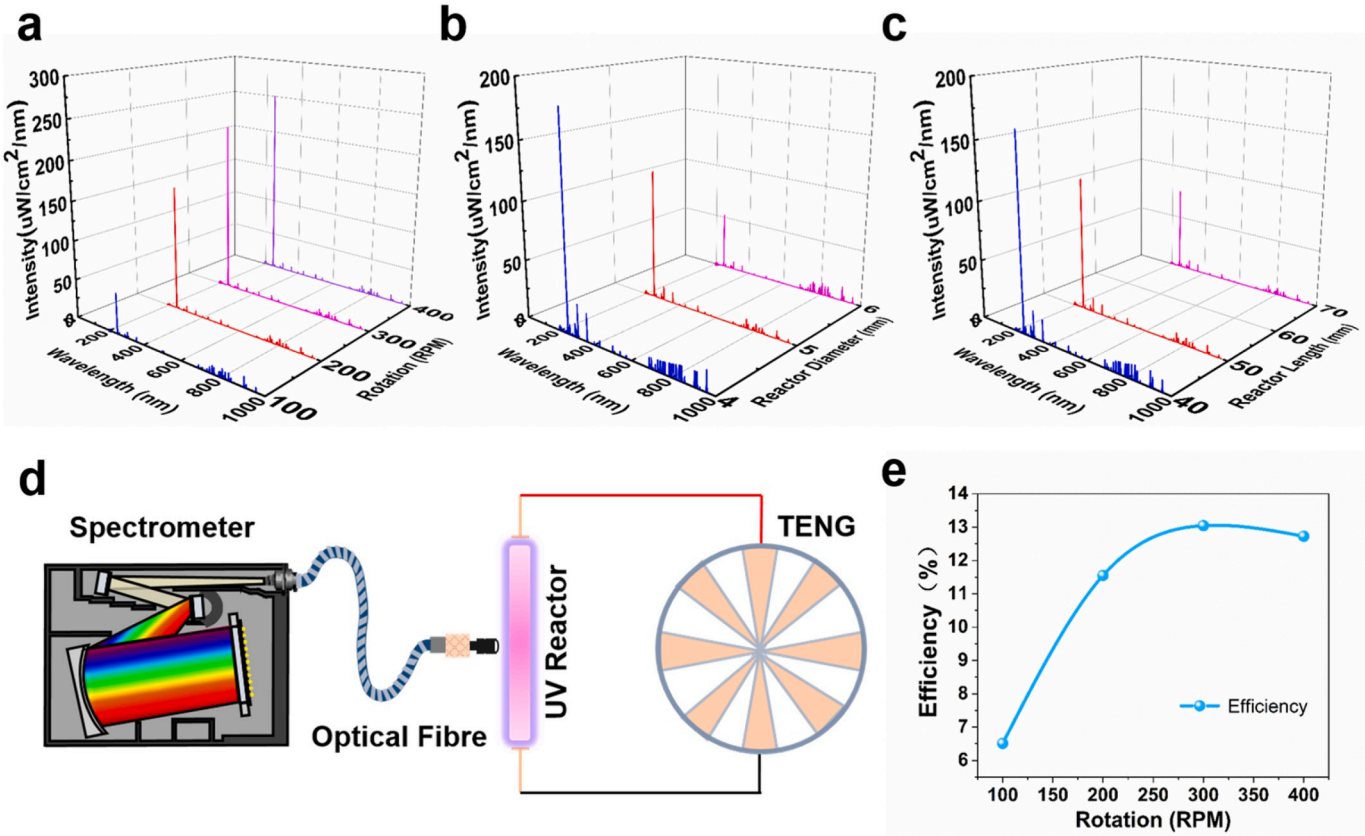

Fig. 3. Optical spectra characteristics of Mobile-UV. (a). The Absolute spectral of the Mobile-UV at different rotational speeds. (b). Absolute spectral of the Mobile-UV at different tube diameters. (c). Absolute spectral of the Mobile-UV at different tube lengths. (d). Schematic measuring Optical spectra characteristics of Mobile-UV. (e). The photoelectric conversion efficiency of Mobile-UV.

bacteria were conducted at one wavelength, 254 nm. Because this wavelength is near the peak of DNA absorption for bacteria [54]. So the ultraviolet light with the main wavelength of 253 nm is exactly what we use for sterilization. Then, the effects on the absolute strength of the UV tube in length and diameter were investigated. The experimental results are shown in Fig. 3 (b) (c). It can be seen that the absolute light intensity emitted by the UV tube has a significant attenuation with the increasing diameter (from 4 to 6 mm), and the lowest value is 50 μW/cm^2/nm. The absolute intensity of the UV tube is also weaker with increasing length (from 40 to 70 mm), with a minimum of 75 μW/cm^2/nm. It is worth noting that the change in diameter and length of the UV tube does not affect the apparent peak intensity at 253 nm. The fixed TENG structure and speed make the power input to UV tubes of different sizes almost the same. As the diameter and length of the UV tube increase, the volume inside the lamp tube will increase accordingly, which will reduce the light energy per unit volume. The optical fiber probe is concentrated at a point in the middle of the tube when measuring, so the measurement value will decrease as the diameter and length of the UV tube increase. Except for a few 700–900 nm infrared bands generated by Ar discharge, most of the converted light energy is concentrated near the UVC band of 253 nm. It indirectly illustrates the high efficiency of UV light produced by Mobile-UV, which will provide data support for applications of Mobile-UV in the future.

Specific experiment methods, such as Fig. 3 (d), were used to measure the absolute spectral intensity of Mobile-UV at different rotational speeds using spectral detection equipment under the conditions of good darkroom environment. Since the previous research did not set any evaluation standard for the efficiency of triboelectric ultraviolet light sources generation, in order to quantitatively analyze the efficiency of Mobile-UV, we propose the efficiency η to evaluate the Mobile-UV, in detail $\eta = \frac{P_{UV}}{P_E} = \frac{I_0 2\pi r L}{UI}$. Among them, P_{UV} is the light power of the ultraviolet tube, P_E is the output electric power of the FR-TENG, I_0 is the absolute intensity of the ultraviolet light emitted by the UV tube. Because the size of the UV tube is short, I_0 is regarded as a constant under the model of assuming the tube as a line source. r, $L$is the diameter, length of the UV tube, respectively. U , I is the load voltage, current of the UV tube. It is not difficult to see from Fig. 3 (e) that as the speed increases, the efficiency will change significantly. It will lay the evaluation standard and theoretical foundation for the optimization research of the Mobile-UV in the future.

2.4. Simulation of triboelectric ultraviolet plasma radiation

In essence, Ultraviolet is the photon radiation produced by electron transition during plasma discharge. Therefore, the performance of plasma glow discharge will directly affect the intensity of Mobile-UV. In order to further study the properties of plasma glow discharge of Mobile-UV, the method of using COMSOL to simulate the entire discharge process is introduced. As shown in Fig. 4 (a), the left side of the symmetrical structure is the real photo of the glow discharge time of the device, and the right side is the electron density distribution map at the discharge moment obtained by COMSOL plasma simulation. It shows that the simulation using COMSOL has good agreement and effectiveness. From the distribution map, it can be seen that the electron density is close to 2×10^{15}/m^3 at the time of discharge. With the help of the plasma module in COMSOL Multiphysics, the simulation parameters are set according to the actual experimental conditions, and the simulation of the discharge process in a cycle (f = 6 Hz, T = 0.016 s) is realized. The specific setup in the COMSOL model is shown in **Supplementary note 4**. The result of the simulated current agrees well with the actual measured current, as shown in Fig. 4 (b). In addition, we get the time-domain distribution of the main plasma parameters (Potential of

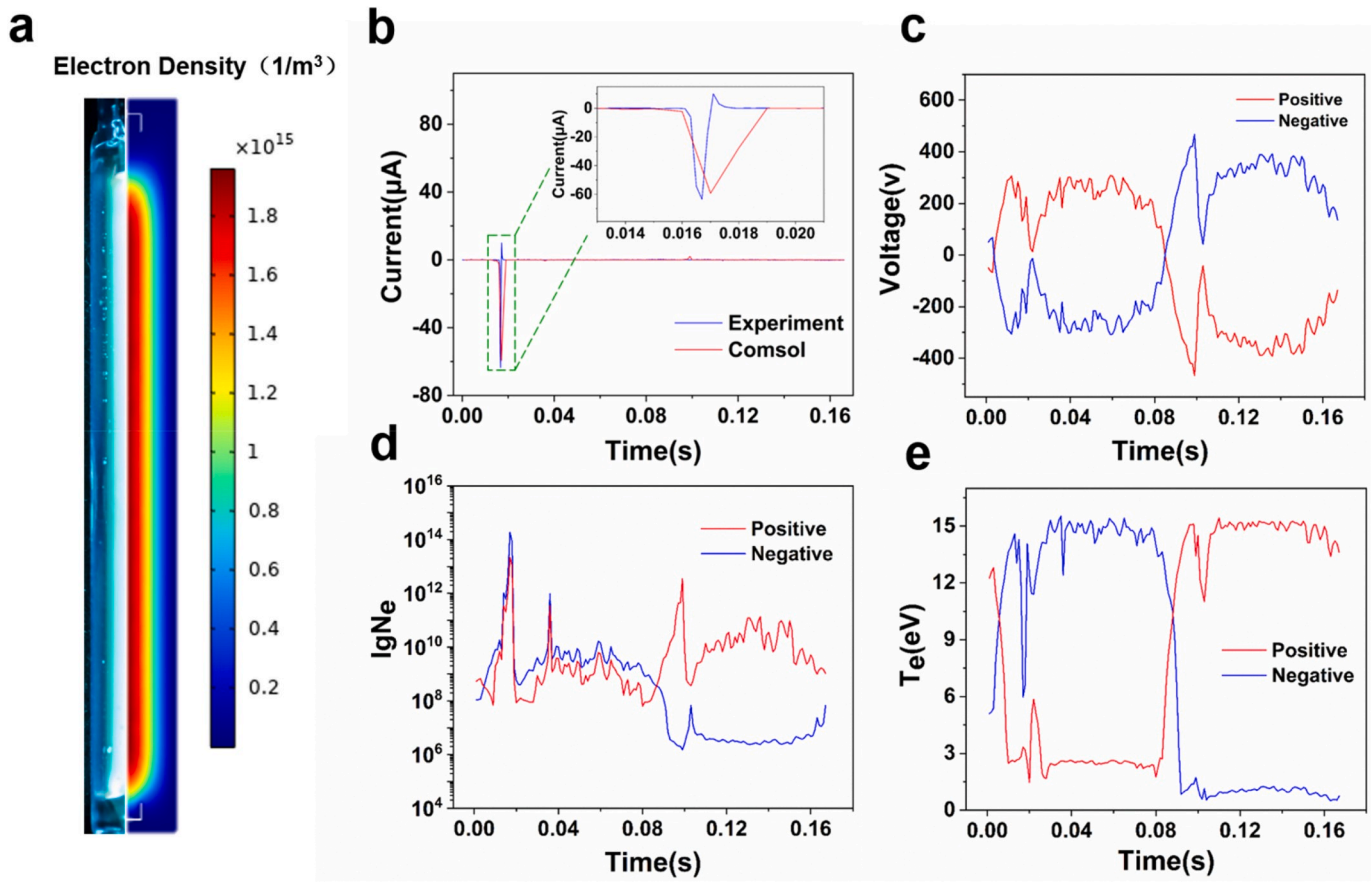

Fig. 4. Simulation of triboelectric ultraviolet plasma radiation. (a). The real photos and simulation results at the moment of discharge. (b). Comparison of simulated current and actual measured current. The inset shows details of current comparison at the discharge moment (c). Voltage changes at the anode and cathode terminals in one cycle (d) (e). Number and Temperature of Electrons changes at the anode and cathode terminals in one cycle.

Plasma, Density of Electrons, and Temperature of Electrons, etc.) in the quartz glass tube. The actual voltage of the electrode can be seen that there is a positive and negative alternating situation between 0 and 0.166 s, and a sudden voltage drop occurs at 0.016 s, as shown in Fig. 4 (c). It can be seen from Fig. 4 (d) that a pulse value appears in the number of electrons, which proves that a glow discharge phenomenon occurred at this moment. Fig. 4 (e) shows the change of the electron temperature at the time of discharge. The electron temperature will change with the alternating voltage load on the electrodes whose highest value can reach 15 eV. The Density and Temperature of Electrons along the axis inside of the tube from positive to the negative electrode are shown in Supplementary note 5. The Density of Electrons changes in a full cycle is shown in Supplementary Movie 2.

Supplementary video related to this article can be found at https://doi.org/10.1016/j.nanoen.2020.104910

2.5. Applications in bio-sterilization, chemical detection, and UV-curing

Mobile-UV can be used in most applications where traditional UV could be used for. For example, bio-sterilization is widely recognized for its stability, safety, low consumption, and high efficiency in water treatment. The application of Mobile-UV in water sterilization has been deeply explored. The whole Mobile-UV sterilization system is shown in Fig. 5 (a). The system mainly includes three modules: FR-TENG as the power supply module, UV sterilizer as the ultraviolet sterilization module and peristaltic pump as the liquid delivery module 1×10^8 CFU/ml *E. coli* solution flowed through the Mobile-UV sterilization tube at the flow rate of 0.5 ml/min by a peristaltic pump. At the same time, the output electrodes of FR-TENG are directly connected with the two electrodes of the Mobile-UV without additional complicated circuits. When FR-TENG and peristaltic pump are started simultaneously, the UV sterilizer is in the actual working state. At this time, the water will be treated in the process of passing through the UV sterilizer and flow into the clean sterile liquid container. The specific experimental process is shown in Fig. 5 (b). According to the above analysis of the intensity of the Mobile-UV system, it was known that the system has the highest intensity at the speed of 400 RPM for FR-TENG. So this rotational speed was set as the working speed of the sterilization experiment. Two different structure sterilizers were designed for Bio-sterilization, such as Fig. 5 (c). The left figure is named Pass-flow Sterilizer (PfS) which the U-type UV reactor is covered by the sterilizing liquid and the reaction-liquid layer is parallel to the UV reactor from the luminescence photograph; The right picture is named Spiral Sterilizer (SpS) where a spiral pipeline is included in, and as is shown in the working statement of the SpS, this spiral pipe is covered by the generated ultraviolet rays, and the specific structure of the two UV reactors is presented in Supplementary note 6. The two types of UV sterilizers are characterized in that there is only a thin layer of high-transparent quartz glass between the ultraviolet light and the liquid to be treated, which minimizes the attenuation rate of ultraviolet rays and improves the sterilization effect for Mobile-UV. As shown in Fig. 5 (d), the sterilization rate of the PfS at working speed can reach 80%, and the sterilization rate of the SpS is 30%. The above sterilization rate is the case where the solution is coated plate immediately after sterilization. Considering the influence of the nutrients in the medium on the reactivation of *E. coli* may lead to a decrease in the sterilization rate, an experiment in which the plated count placed in the PfS solution for 1 h later was designed to eliminate the above-mentioned influencing factors, and the bactericidal rate was 89%.

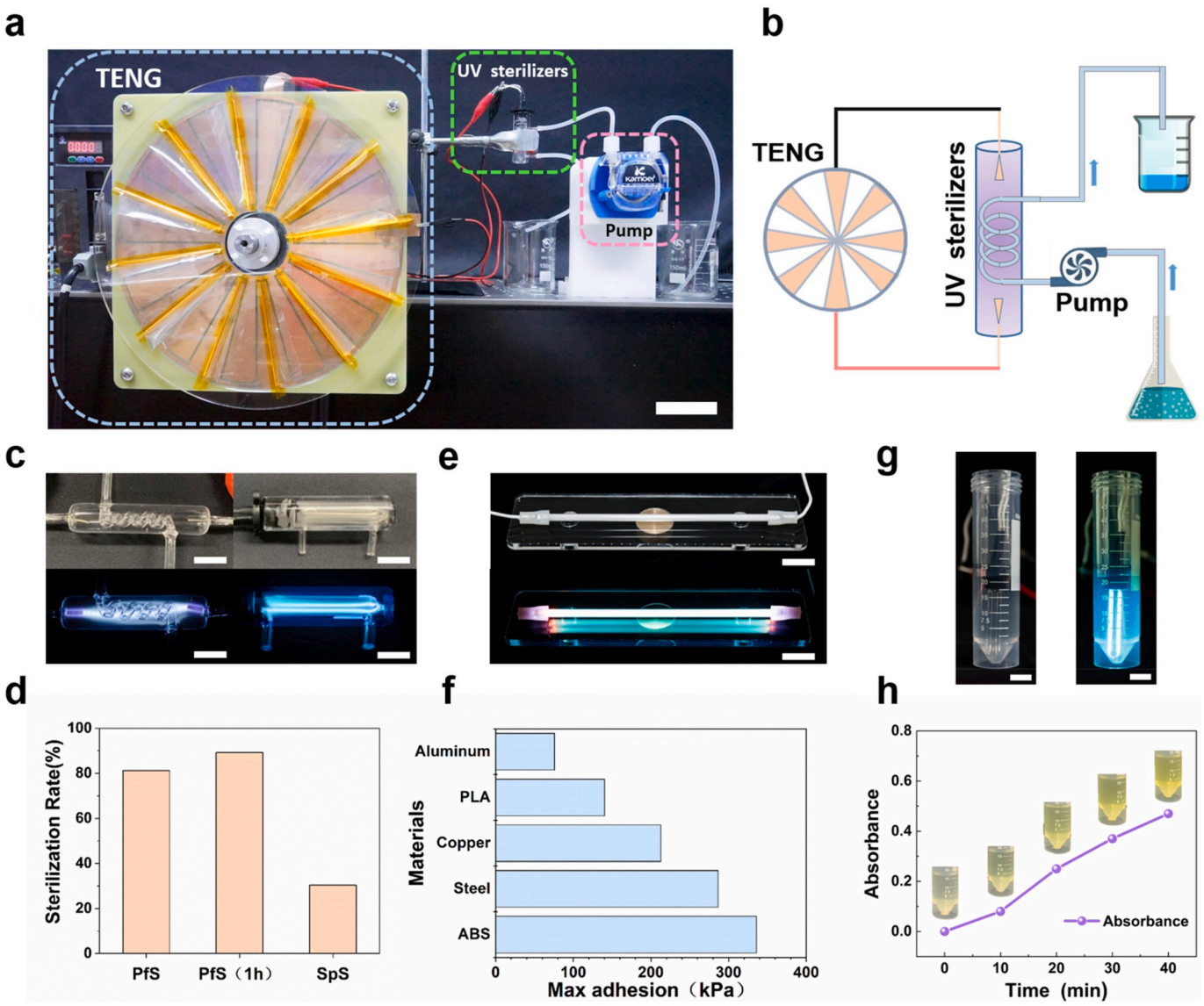

Fig. 5. Application in Bio-sterilization, Chemical detection, and UV-curing. (a). Photograph of whole Mobile-UV water sterilization system (scale bar, 70 mm) (b). Schematic diagram of the Mobile-UV water sterilization. (c). The Luminescence photographs of different Mobile-UV water Sterilizers (scale bar, 15 mm). (d). The sterilization rate of different Sterilizers. (e). Photograph of Mobile-UV in curing (scale bar, 20 mm). (f). The maximum adhesion of different materials by Mobile-UV curing (g) Photograph of Mobile-UV for chemical detection. (scale bar, 10 mm). (h)The absorbance of $KI-KIO_3$ mixed solution with the accumulation of exposure time by Mobile-UV.

In addition to biological sterilization, Mobile-UV can also be applied to curing. It will provide new methods and approaches for UV-curing applications, which will greatly increase the possibility of ultraviolet in lean and backward areas. The experiments to verify the effect of UV-curing were designed as shown in Fig. 5 (e). The difference in curing materials is usually a challenge for Mobile-UV. Therefore, we applied a layer of UV-curing glue to the surface of a cylindrical block (diameter is 20 mm) which was made of different materials (aluminum, copper, steel, PLA, ABS) and attached it to a transparent acrylic sheet (thickness is 5 mm), and then we irradiated it by this system. Finally, we measured the maximum adhesion (the maximum tensile force required to separate the cylindrical block from the acrylic plate) after irradiation, the maximum adhesion of different materials is shown in Fig. 5 (f). The force measuring device and process is presented in Supplementary note 7 and the curing process by Mobile-UV is shown in Supplementary Movie 1.

Similarly, in order to verify that Mobile-UV can also be used in the field of chemical detection, previous studies have shown that UV radiation can produce photochemical reactions in $KI-KIO_3$ solutions [55–58](The principle of the chemical reaction is presented in Supplementary note 7.) This chemical reaction will affect the absorbance in 352 nm (A352) of the $KI-KIO_3$ solutions. Therefore, the Mobile-UV reactor was placed in a plastic tube containing the $KI-KIO_3$ mixed solution, as shown in Fig. 5 (g). This system irradiated the mixed solution for 10, 20, 30, and 40 min at 400 RPM for FR-TRNG, respectively. Using the absorbance of the unexposed solution as the background, we detected the A352 of the treated solution by UV spectrophotometer. The results from Fig. 5 (h) shown that the deeper the photochemical reaction is, the higher the concentration of I_3^- in the solution is with the accumulation of irradiation time, so the color of solutions was deepened correspondingly. This successful application shows that Mobile-UV can be applied to photochemical reactions, which provides a new way to produce UV in photochemical applications. The chemical reaction process in detail is shown in Supplementary Movie 1.

3. Conclusions

In this paper, we proposed the Mobile-UV which utilizes the natural characteristic high-voltage output of TENG, and generates Mobile ultraviolet light sources without any external circuit. For this system, electric and spectral characteristics were analyzed, respectively. The results showed that as the speed accelerated, the discharge current of the two electrodes increased and the load voltage decreased. It was observed that the efficiency of photoelectric conversion for UV tube would be improved with the increase of rotational speed. Factor experiments about different sizes were conducted to obtain the change rule of light intensity. The simulation under COMSOL was conducted to study the underlying mechanisms of Mobile-UV in the plasma field, the experiment and simulation were in well agreement. Finally, the applications in bio-sterilization, chemical detection, and UV-curing verified the great advantage as Mobile ultraviolet light sources. Taking natural advantage, high voltage, low current and charge, this technology broadens the field of high voltage applications of TENG. We believe that it will promote the application of ultraviolet light in wild sterilization, wound treatment, chemical detection, medical diagnosis, and even 3D light-curing printing. Recently, the highly infectious coronavirus COVID-19 respiratory disease is sweeping the globe, which results in more demand for often disinfection and sterilization of public facilities, such as door handles or faucet handles, *etc*. The Mobile-UV might be a promising technology for converting the mechanical energy of door opening or water flowing to UV radiation in the condition mentioned above.

4. Methods

4.1. Structural design of FR-TENG

FR-TENG includes the TENG rotor, nylon layer, TENG stator, and TENG support plate. The TENG stator (300 mm × 300 mm × 2 mm) material is a PCB board, and the surface is plated with a grid-shaped copper electrode. The positive and negative electrodes are alternately distributed, and the positive and negative electrode spacing is 5 mm. The TENG stator and the TENG support plate (300 mm × 300 mm x 5 mm) with mounting holes were joined together by screws and nuts through openings arranged at the four corners. Then, a nylon layer having a diameter of 290 mm and a thickness of 0.05 mm was adhered to the surface of the TENG stator using double-sided tape. The TENG rotor consists of a rotating disc with a PVC sheet film attached to it. The disc is made of an acrylic sheet with a diameter of 330 mm and a thickness of 5 mm. The surface is engraved with a pair of narrow rectangular through grooves. One end of the sheet-like PVC film with a thickness of 0.1 mm is adhered to the rectangle of the acrylic disc by Kapton tape. Inside the tank, the other end of the PVC membrane is free to float. With the aid of a flange, the TENG rotor fits snugly against the nylon layer.

4.2. Electrical, optical emission measurement

The Keithley 6514 electrometer was used as an electric measuring device with an internal resistance of about 200 TΩ. The voltage or current can be selected by switching between different gears. The Keithley 6514 electrometer is used to measure the voltage in series with the PINTECH HVP-40 high voltage probes which impedance is 1 GΩ. The AvaSpec-HSC1024x58TEC-EVO was used as an optical emission measuring device with a spectral range of 200–1160 nm and a signal-to-noise ratio of 1200:1.

4.3. Bacterium cultivation

Escherichia coli strains were purchased from the China Center of Industrial Culture Collection (CICC). According to the strains provided by CICC, the medium components were beef extract 10.0g, peptone 10.0g, glucose 10.0 g, NaCl 5.0 g, agar 15.0–20.0 g, distilled water 1.0 L, pH 7.0, and the culture temperature was 35 °C.

4.4. Material preparation of $KI - KIO_3$

9.96 g *KI*, 2.14 gKIO_3 and 0.38 g $Na_2B_4O_7{\cdot}10H_2O$ were weighed using a precision digital balance, dissolved in deionized water, and shaken. *KI*, KIO_3supplied by Xilong Scientific, $Na_2B_4O_7{\cdot}10H_2O$ supplied by Beijing Chemical Plant, purity purely analytical. The UV spectrophotometer model is the Ultrospec 9000 produced by GE, and the instrument is provided by the Protein Research Technology Center of Tsinghua University.

4.5. UV-curing experiments

The UV-curing glue used in the experiment was K2018 produced by KSIMI with a curing band of 200–400 nm. The UV-curing lamp used in the experiment had a wavelength of 365 nm. The force sensor used in the detection device for quantifying the Mobile-UV curing effect is SBT671, produced by SimBatouch Electronic Technology.

Data availability

The data that support the plots within this paper and other findings of this study are available from the corresponding author upon reasonable request.

Author contributions

Z. W. and Y. S. contribute equally to this work. Z. W., J. C., and Z. L. Wang conceived the idea and guided the project. Z. W., Y. S., and J. C. were in charge of the overall design and fabrication of the devices, experiments, data gathering and analysis, F. L., R. S., contributed with ideas for experimental design and assisted with design and manufacture of the device. H. W., X. L., Y. L. assisted with the electric measurement and design of applications. L. J. contributed to the whole experimental guidance and supplement. All the authors discussed the data and prepared the manuscript.

Declaration of competing interest

The authors declare that they have no known competing financial interests or personal relationships that could have appeared to influence the work reported in this paper.

CRediT authorship contribution statement

Zhaozheng Wang: Conceptualization, Methodology, Writing - review & editing. **Yunxu Shi:** Formal analysis, Methodology. **Fan Liu:** Formal analysis. **Hao Wang:** Data curation. **Xu Liu:** Data curation. **Runtong Sun:** Investigation. **Yijia Lu:** Software. **Linhong Ji:** Project administration. **Zhong Lin Wang:** Validation, Supervision. **Jia Cheng:** Conceptualization, Supervision, Validation.

Acknowledgments

This work was supported by the National Science and Technology Major Project of China (Grant No. 2011ZX02403), the National Key Research and Development Program of China (No. 2018YFF0300606), the National Natural Science Foundation of China (No. U1613207) and the Tsinghua University Initiative Scientific Research Program (No. 20193080001), The Graduate Innovation Foundation of YanTai University (No. YDZD1907).

Appendix A. Supplementary data

Supplementary data to this article can be found online at https://doi.

org/10.1016/j.nanoen.2020.104910.

References

[1] G. Ruiters, Electric Capitalism: Recolonising Africa on the Power Grid, 2009, 248e264.
[2] G. Ruiters, Afr. Dev. 36 (2011) 119–142.
[3] J. Jeong, C. Kim, J. Yoon, Water Res. 43 (2009) 895–901.
[4] C.A. Martínez-Huitle, E. Brillas, Angew. Chem. Int. Ed. 47 (2008) 1998–2005.
[5] L.-S. Wang, H.-Y. Hu, C. Wang, Environ. Sci. Technol. 41 (2007) 160–165.
[6] U. Von Gunten, Water Res. 37 (2003) 1469–1487.
[7] W.A. Rutala, D.J. Weber, Clin. Microbiol. Rev. 10 (1997) 597–610.
[8] S.W. Krasner, J.M. Wright, Water Res. 39 (2005) 855–864.
[9] T.F. Clasen, D.H. Thao, S. Boisson, O. Shipin, Environ. Sci. Technol. 42 (2008) 4255–4260.
[10] T. Justel and C. Feldmann, Radiation Therapy and Medical Imaging Using UV Emitting Nanoparticles U.S. Patent Application No. 10/596, 440, 2007.
[11] W. Westerhof, L. Nieuweboer-Krobotova, Arch. Dermatol. 133 (1997) 1525–1528.
[12] C.S. Dulcey, J.H. Georger, V. Krauthamer, D.A. Stenger, T.L. Fare, J.M. Calvert, Science 252 (1991) 551–554.
[13] M. Invernizzi, G. Natale, M. Levi, S. Turri, G. Griffini, Materials 9 (2016) 583.
[14] Z.-H. Liang, Y. Cheng, W. Hsu, Y.-W. Lee, in: 2004 Proceedings. 54th Electronic Components and Technology Conference (IEEE Cat. No. 04CH37546), IEEE, 2004, pp. 1486–1491.
[15] S. Li, H. Boyter, N. Stewart, AATCC Rev. (2004) 4.
[16] F.-R. Fan, Z.-Q. Tian, Z. Lin Wang, Nano Energy 1 (2012) 328–334.
[17] F.R. Fan, W. Tang, Z.L. Wang, Adv. Mater. 28 (2016) 4283–4305.
[18] Y. Zi, H. Guo, Z. Wen, M.-H. Yeh, C. Hu, Z.L. Wang, ACS Nano 10 (2016) 4797–4805.
[19] C. Zhao, Q. Zhang, W. Zhang, X. Du, Y. Zhang, S. Gong, K. Ren, Q. Sun, Z.L. Wang, Nano Energy 57 (2019) 440–449.
[20] W. Zhong, L. Xu, H. Wang, J. An, Z.L. Wang, Adv. Funct. Mater. (2019), 1905319.
[21] T. Liu, M. Liu, S. Dou, J. Sun, Z. Cong, C. Jiang, C. Du, X. Pu, W. Hu, Z.L. Wang, ACS Nano 12 (2018) 2818–2826.
[22] P. Wang, L. Pan, J. Wang, M. Xu, G. Dai, H. Zou, K. Dong, Z.L. Wang, ACS Nano 12 (2018) 9433–9440.
[23] K. Dong, J. Deng, W. Ding, A.C. Wang, P. Wang, C. Cheng, Y.C. Wang, L. Jin, B. Gu, B. Sun, Adv Energy Mater 8 (2018), 1801114.
[24] W. Ding, J. Zhou, J. Cheng, Z. Wang, H. Guo, C. Wu, S. Xu, Z. Wu, X. Xie, Z. L. Wang, Adv Energy Mater 9 (2019).
[25] S. Xu, W. Ding, H. Guo, X. Wang, Z.L. Wang, Adv Energy Mater 9 (2019).
[26] R. Lei, H. Zhai, J. Nie, W. Zhong, Y. Bai, X. Liang, L. Xu, T. Jiang, X. Chen, Z. L. Wang, Adv Mater Technol 4 (2019), 1800514.
[27] Z.L. Wang, Nature 542 (2017) 159–160.
[28] Y. Xi, H. Guo, Y. Zi, X. Li, J. Wang, J. Deng, S. Li, C. Hu, X. Cao, Z.L. Wang, Adv Energy Mater 7 (2017), 1602397.
[29] X. Li, J. Tao, X. Wang, J. Zhu, C. Pan, Z.L. Wang, Adv Energy Mater 8 (2018), 1800705.
[30] J. Wang, L. Pan, H. Guo, B. Zhang, R. Zhang, Z. Wu, C. Wu, L. Yang, R. Liao, Z. L. Wang, Adv Energy Mater 9 (2019), 1802892.
[31] X. Liang, T. Jiang, G. Liu, T. Xiao, L. Xu, W. Li, F. Xi, C. Zhang, Z.L. Wang, Adv. Funct. Mater. (2019), 1807241.
[32] J. Chen, H. Guo, Z. Wu, G. Xu, Y. Zi, C. Hu, Z.L. Wang, Nano Energy 64 (2019), 103920.
[33] H. Guo, X. Pu, J. Chen, Y. Meng, M.-H. Yeh, G. Liu, Q. Tang, B. Chen, D. Liu, S. Qi, Sci Robotics 3 (2018) eaat2516.
[34] X. Zhang, M. Yu, Z. Ma, H. Ouyang, Y. Zou, S.L. Zhang, H. Niu, X. Pan, M. Xu, Z. Li, Adv. Funct. Mater. (2019), 1900327.
[35] H. Ouyang, Z. Liu, N. Li, B. Shi, Y. Zou, F. Xie, Y. Ma, Z. Li, H. Li, Q. Zheng, Nat. Commun. 10 (2019) 1821.
[36] Z. Liu, Y. Ma, H. Ouyang, B. Shi, N. Li, D. Jiang, F. Xie, D. Qu, Y. Zou, Y. Huang, Adv. Funct. Mater. 29 (2019), 1807560.
[37] J. Chen, B. Chen, K. Han, W. Tang, Z.L. Wang, Adv Mater Technol (2019), 1900337.
[38] W. Ding, C. Wu, Y. Zi, H. Zou, J. Wang, J. Cheng, A.C. Wang, Z.L. Wang, Nano Energy 47 (2018) 566–572.
[39] M. Xu, Y.-C. Wang, S.L. Zhang, W. Ding, J. Cheng, X. He, P. Zhang, Z. Wang, X. Pan, Z.L. Wang, Extreme Mech Letts 15 (2017) 122–129.
[40] Z. Wu, W. Ding, Y. Dai, K. Dong, C. Wu, L. Zhang, Z. Lin, J. Cheng, Z.L. Wang, ACS Nano 12 (2018) 5726–5733.
[41] C. Wu, W. Ding, R. Liu, J. Wang, A.C. Wang, J. Wang, S. Li, Y. Zi, Z.L. Wang, Mater. Today 21 (2018) 216–222.
[42] W. Ding, A.C. Wang, C. Wu, H. Guo, Z.L. Wang, Adv Mater Technol (2019) 4.
[43] C.-M. Chiu, Y.-Y. Ke, T.-M. Chou, Y.-J. Lin, P.-K. Yang, C.-C. Wu, Z.-H. Lin, Nano Energy 53 (2018) 1–10.
[44] C.M. Chiu, S.W. Chen, Y.P. Pao, M.Z. Huang, S.W. Chan, Z.H. Lin, Sci. Technol. Adv. Mater. 20 (2019) 964–971.
[45] Y.-H. Tsao, R.A. Husain, Y.-J. Lin, I. Khan, S.-W. Chen, Z.-H. Lin, Nano Energy 62 (2019) 268–274.
[46] Y.-J. Fan, M.-Z. Huang, Y.-C. Hsiao, Y.-W. Huang, C.-Z. Deng, C. Yeh, R.A. Husain, Z.-H. Lin, Nano Energy 69 (2020).
[47] F. Liu, Y. Liu, Y. Lu, Z. Wang, Y. Shi, L. Ji, J. Cheng, Nano Energy 56 (2019) 482–493.
[48] J. Cheng, W. Ding, Y. Zi, Y. Lu, L. Ji, F. Liu, C. Wu, Z.L. Wang, Nat. Commun. 9 (2018) 3733.
[49] Y. Zi, C. Wu, W. Ding, X. Wang, Y. Dai, J. Cheng, J. Wang, Z. Wang, Z.L. Wang, Adv. Funct. Mater. 28 (2018), 1800610.
[50] A. Li, Y. Zi, H. Guo, Z.L. Wang, F.M. Fernandez, Nat. Nanotechnol. 12 (2017) 481–487.
[51] C. Wu, H. Tetik, J. Cheng, W. Ding, H. Guo, X. Tao, N. Zhou, Y. Zi, Z. Wu, H. Wu, Adv. Funct. Mater. (2019), 1901102.
[52] H. Huo, F. Liu, Y. Luo, Q. Gu, Y. Liu, Z. Wang, R. Chen, L. Ji, Y. Lu, R. Yao, J. Cheng, Nano Energy 67 (2020), 104150.
[53] C.B. Han, C. Zhang, J. Tian, X. Li, L. Zhang, Z. Li, Z.L. Wang, Nano Res 8 (2015) 219–226.
[54] T.P. Coohill, J.L. Sagripanti, Photochem. Photobiol. 84 (2008) 1084–1090.
[55] R.O. Rahn, Photochem. Photobiol. 66 (1997) 450–455.
[56] J.R. Bolton, K.G. Linden, J. Environ. Eng. 129 (2003) 209–215.
[57] R.O. Rahn, M.I. Stefan, J.R. Bolton, E. Goren, P.S. Shaw, K.R. Lykke, Photochem. Photobiol. 78 (2003) 146–152.
[58] S. Jin, A.A. Mofidi, K.G. Linden, J. Environ. Eng. 132 (2006) 831–841.